


## Research

# Enhancement of gold-curcumin nanoparticle mediated radiation response for improved therapy in cervical cancer: a computational approach and predictive pathway analysis

Priya Yadav<sup>1,2</sup> · Arghya Bandyopadhyay<sup>1,3</sup>  · Keka Sarkar<sup>1</sup> 

Received: 27 March 2024 / Accepted: 5 September 2024

Published online: 18 September 2024

© The Author(s) 2024 

## Abstract

Radiotherapy is prevalently applied for highly effective cancer therapy while the low specificity of radiation is deleterious to the nearby healthy cells. High-Z-based nanomaterials offer excellent radio-enhancement properties while natural products provide radioprotection. Modulation of the radiotherapeutic index via applying nanomaterials is feasible for effective treatment however, the scenario changes when simultaneous protection of non-cancerous cells is required. Here, we report the modulatory radiotherapeutic effect of curcumin conjugated gold nanoparticles in a single nanoformulation to pave the long-awaited hope of a *single combination-based, cell-selective radio enhancer, and protectant for cancer radiotherapy*. We have validated the effective radiation dose along with the combination of the radio-nano-modulator by a reverse experimentation statistical model. The concept was supported by different sets of experiments, like quantification of ROS generation, cell cycle monitoring, mitochondrial membrane potential measurement, etc. along with *gene expression* study, and predictive modeling of molecular pathways of the killing mechanism. In conclusion, the nanoconjugate showed a promise to become a candidate for the pH-dependent cell-specific radio-modulator.

**Keywords** Gold-curcumin nanoparticles · Metal-phytodrug nanoconjugates · Ionizing radiation · Radiosensitization · Radioprotection · Oxidative stress · Programmed cell death

## 1 Introduction

Radiation therapy is the foremost chosen method for the treatment of locally advanced cancers. While radiation therapy contributes to severe deleterious effects on neighboring non-cancerous cells. Radiation therapy also potentially influences immune suppression, and bone marrow degradation [1]. To minimize the deleterious effects of radiation, radio-ligand therapy (RLT) or radionuclide therapy is a better choice over conventional radiation treatment [2]. Radionuclide therapy delivers radionuclides close to the site hence significantly lowering the adverse effect of radiation damage to normal local tissues [3]. During RLT, the healthy local tissues around the tumor tend to receive a prolonged radiation

---

Priya Yadav and Arghya Bandyopadhyay contributed equally.

**Supplementary Information** The online version contains supplementary material available at <https://doi.org/10.1186/s11671-024-04104-7>.

✉ Arghya Bandyopadhyay, [arghya.micro@gmail.com](mailto:arghya.micro@gmail.com); ✉ Keka Sarkar, [keka@klyuniv.ac.in](mailto:keka@klyuniv.ac.in) | <sup>1</sup>Department of Microbiology, University of Kalyani, Kalyani, West Bengal 741235, India. <sup>2</sup>Department of Biochemistry and Biotechnology, Annamalai University, Annamalai Nagar, Tamil Nadu 608002, India. <sup>3</sup>Department of Nanoscience and Nanotechnology, University of Kalyani, Kalyani, West Bengal 741235, India.



dose due to the presence of radionuclides within the body. Unfortunately, traditional radiation therapy as well as RLT bombards the system with high-energy radiation doses [4, 5]. Alternatively, Auger therapy relies on low-energy electrons for the treatment of cancer where the presence of a metal within the cell is capable of releasing Auger electrons upon being charged by external radiation. The Auger therapy is low low-energy method for damaging cancer cells unlike conventional radiation therapy consequently it can be implied as the next generation of cancer radiation therapy [6–8]. The Auger therapy can be tailored for targeting cancer cells by combining the electron emitter with a homing ligand molecule. Auger therapy is an attractive approach to treating cancer by damaging the DNA and arresting cell division thereby halting tumor growth and metastases [9]. Unlike conventional radiation therapy, during Auger therapy, the applied radiation dose can be minimized due to the presence of ligands. Moreover, the high Z metals are considered a true magic bullet in Auger therapeutics [10]. For instance, the case of cisplatin served as a potential chemotherapeutic for cancer therapy where metallic parts along with organic effectors are responsible for the potency of cisplatin [11]. However, due to the high energy covalent bonds between metal and organic moiety present in the cisplatin tends to be highly toxic for normal cells as they cannot be metabolized easily nor can be cleared from the system [12].

Metallic gold nanomaterials, due to their inherent chemical stability and excellent biocompatibility, have been utilized for various biomedical applications such as tagging cells and proteins, delivering therapeutic agents [13] and/or drugs, ultrasensitive detection of biomolecules [14], radiosensitizer [15] or radio-enhancers [16]. Gold nanomaterials are also employed for photodynamic therapy [17] and the most recent hyperthermic treatment [18]. Gold nanoparticles (AuNPs) act as an excellent radiosensitizing agent and assist in effective radiation therapy due to increased photoelectric absorption of (radiation) cross-sections relative to tissue [19, 20]. AuNPs along with ionizing radiations (IR) contributes to generating enormous reactive oxygen species ( $O^{2-}$ ,  $^1O_2$ , and  $\cdot OH$ ) and are eligible to be potent radiosensitizer [19]. The IRs follow either direct or indirect mechanisms for cellular damage. During direct damage, the radiation knocks the DNA molecule directly and disrupts its molecular structure which leads to cellular death while in the course of indirect radiation damage, the radiation ionizes the aqueous environment of cells and generates highly reactive unpaired free hydroxyl ( $HO\cdot$ ) and alkoxy ( $RO\cdot$ ) radicals which further interact with macromolecules to disrupt its structure thereby impair its functional efficiency and eventually cell death [21–23]. In radiobiology, it has been well established that the majority of radio-mediated damages occur due to indirect action mechanisms since water comprises about 70% of the cellular composition [22]. Cancer cells develop radioresistance by eloping from the intracellular reactive oxygen species (ROS) generated through IRs via manipulating the redox system of cells [24]. Studies have revealed that AuNPs are identified to inhibit thioredoxin reductase (TrxR) and disrupt the cellular redox state via interacting and binding to its selenocysteine-containing active site of the TrxR enzyme. Reduced thioredoxin regulates the apoptosis and protects against oxidative stress. The AuNPs binding with the enzyme is therefore preventing the reduction of thioredoxin and disrupts the redox balance in cells resulting in increased oxidative stress thereby inducing cell death [25–27]. Curcumin, a natural competitive inhibitor occupies the active site of TrxR and this binding induces conformational changes in the structure of the enzyme leading to irreversible inhibition thereby disrupting the redox balance in the cells. Conjugation of curcumin with AuNPs in combination with IR acts as a redox-modulating agent that significantly inhibits the thioredoxin reductase [28–30]. However, the implementation of nanomaterials along with IRs remarkably increases the intracellular ROS levels for a prolonged time thereby compromising the abilities of cancer cells to modulate the redox system [31]. Therefore, the antioxidant blocking is persistent enough to culminate in cell death without providing the opportunity for cancer cells to develop radioresistance [32, 33]. But this resistance mechanism is not effective enough against the Auger electrons generated by the gold NPs upon sensitization with radiation; as the physical mechanism of cell killing is not prone to any cellular resistance since virtually all resistance mechanism develops against certain chemical pathways of cell killing method. As the Auger electron can travel only a very short distance, like a few hundred nanometers only, thus those electrons are only effective to the boundary of the cell and not the neighboring cells, but they can effectively harm the intracellular structures like nucleic acids.

During radiation therapy, the protection of neighboring cells from the damaging effect of IRs is mainly conveyed by radioprotectant compounds. The radioprotectant must be given to cells before or at the time of irradiation. Herbal compounds are revealed to have the aptitude to protect cells against IRs and behave as a potent radioprotector [34]. Numerous natural compounds, such as quercetin, naringin, gallic acid, piperine, and curcumin exhibit persuasive radioprotective properties [35–38]. Interestingly, curcumin is revealed to act as a radiosensitizer in cancerous cells while offering radioprotection in non-cancerous cells [39, 40]. Curcumin, a natural polyphenolic compound, principally exists in keto-enol form, and its biological activities such as antioxidant, anti-inflammatory, antimicrobial, and anticancer properties exclusively depend on its molecular configuration (keto-enol tautomers) depending on intracellular pH conditions. Mainly, the keto form is responsible for the antioxidant properties of curcumin [41, 42]. The mechanism of radioprotection

of curcumin is conferred by the pro-oxidant property, GSH-antioxidant induced response, and cytoprotection *in-vitro*. The chromosome degradation increased significantly in the gamma-irradiated group which was decreased evidently in cells incubated with curcumin. The results demonstrated that the antioxidant properties of curcumin facilitate both protection and chromosome damage repair that caused due to gamma radiation. The anti-lipoperoxidation effect of curcumin could be linked to explain by its direct free radical scavenger property that further confers the radioprotection [43, 44]. Another study demonstrated the improvement in radioprotection efficacy and enhanced survival rate in mice which was pre-incubated with curcumin-conjugated albumin nanoparticles and then given X-ray irradiation [45]. Despite being a safe drug, it endures several inadequacies such as low biological availability, photodegradation, and poor pharmacokinetics that can be rectified efficiently with the aid of nanotechnology [35, 46].

Considering above mentioned facts, we have developed a curcumin-coated gold nanoparticle system for the validation of our concept of a single combination having both radio sensitization and radio protectant properties in a cell-selective manner. Since the late 1970s, different research groups explored structurally dissimilar molecules and their combination to be employed as either radioprotector for non-cancerous cells or radio-enhancer for cancerous cells but failed due to the non-selective behavior of the molecules used [47–50]. To the best of our knowledge, this is the first study to demonstrate a single (nano)formulation based on the combination of gold and curcumin that provides a higher radiotherapeutic index in cancer cells (HeLa cell line) along with the potential to have radiation protection to non-cancerous cells (HEK-293 cell line) selectively. Thus, the present study revealed the role of metal-based radiosensitizers alone or in combination with phytochemicals to be validated for their preferential translation into clinical developments for next-generation radiation-mediated cancer therapy with minimal repercussions.

## 2 Results and discussion

### 2.1 Preparation and characterization of NPs

The curcumin-conjugated gold nanoparticles (AuCur NPs) were synthesized by the chemical reduction and nucleation method. During the synthesis process, curcumin acts as a reducing as well as a capping agent. The resultant AuCur NPs suspension was hydrophilic as seen in the inset of Fig. 1a. The UV–vis spectroscopy depicts the absorption spectra of AuCur NPs that revealed two prominent peaks at 376 nm and 539 nm for curcumin and gold NPs respectively (Fig. 1a). Plasmonic properties particularly, localized surface plasmon resonance (LSPR) properties predict the shape and dimension of gold-based nanomaterials. To validate the LSPR properties, the spectral analysis of curcumin (Cur) solution and AuNPs was also conducted separately. The spectral scan of AuNPs had the SPR peak at 525 nm (Additional file 1: Fig. S1a) and the curcumin solution gives the maximum absorption peak at 420 nm (Additional file 1: Fig. S1b) [51, 52]. As it is revealed by a spectral scan of AuCur NPs, there was a blue shift of 53 nm (from 420 to 367 nm) in the absorption spectra of curcumin while a redshift of 14 nm (from 525 to 539 nm) was found in the LSPR band of gold. The change in the spectral scan of AuNPs and curcumin alone as compared to AuCur NPs confirms the possible conjugation of curcumin with AuNPs, which was further confirmed by FT-IR. To confirm the morphology and size of AuCur NPs, HR-TEM and AFM studies were conducted. The HR-TEM micrograph approves a spherical morphology with an average size of  $7 \text{ nm} \pm 2.29 \text{ nm}$  (inset Fig. 1b). The size and shape of the AuCur NPs from AFM analysis signified the spherical morphology. Also, Fig. 1c divulged the 2-D and 3-D distribution of AuCur NPs along with the line analysis of a single NP (Fig. 1c iii & iv), confirming an average size of 5.62 nm with an apparently smooth surface. The AuCur NPs have a hydrodynamic size of  $135 \pm 0.76 \text{ nm}$  (polydispersity index: 0.3) (Fig. 1d i) and the Zeta potential ( $\zeta$ ) measurements revealed that the NPs have fairly good stability with  $\zeta$  value  $-13 \pm 0.23 \text{ mV}$  (Fig. 1d ii). A good zeta potential value is indicative of NPs stability that was previously confirmed by TEM and AFM analysis which showed a fair distribution of NPs without any aggregation. The conjugation and possible interaction of curcumin with the AuNPs surface were studied by FT-IR spectroscopy. During the capping of AuNPs, the hydroxyl groups present in the phenolic and enolic parts of curcumin were involved in interaction and binding with AuNPs. FT-IR spectra showed wider plane bending of the –OH stretching at  $1628$ ,  $1285$ , and  $1153 \text{ cm}^{-1}$  in the curcumin scan. These –OH stretching was observed to be diminished in AuCur NPs spectra due to curcumin's active interaction for binding with AuNPs (Fig. 1e). Moreover the –OH stretching present in AuNPs at  $3495 \text{ cm}^{-1}$  gets broadened in AuCur NPs spectra due to vibrational stretching during the interaction with curcumin. The peaks present at curcumin for –COO<sup>−</sup> stretching, and C–H stretching of aliphatic bonds at  $1754$ ,  $1024$ , and  $962 \text{ cm}^{-1}$  showed planer widening in AuCur NPs confirming the capping of curcumin on AuNPs. The FT-IR data confirms that curcumin was adhered to the surface of gold by the formation of metal–ligand  $\pi$  bonding, facilitated by the presence of a large amount of positive

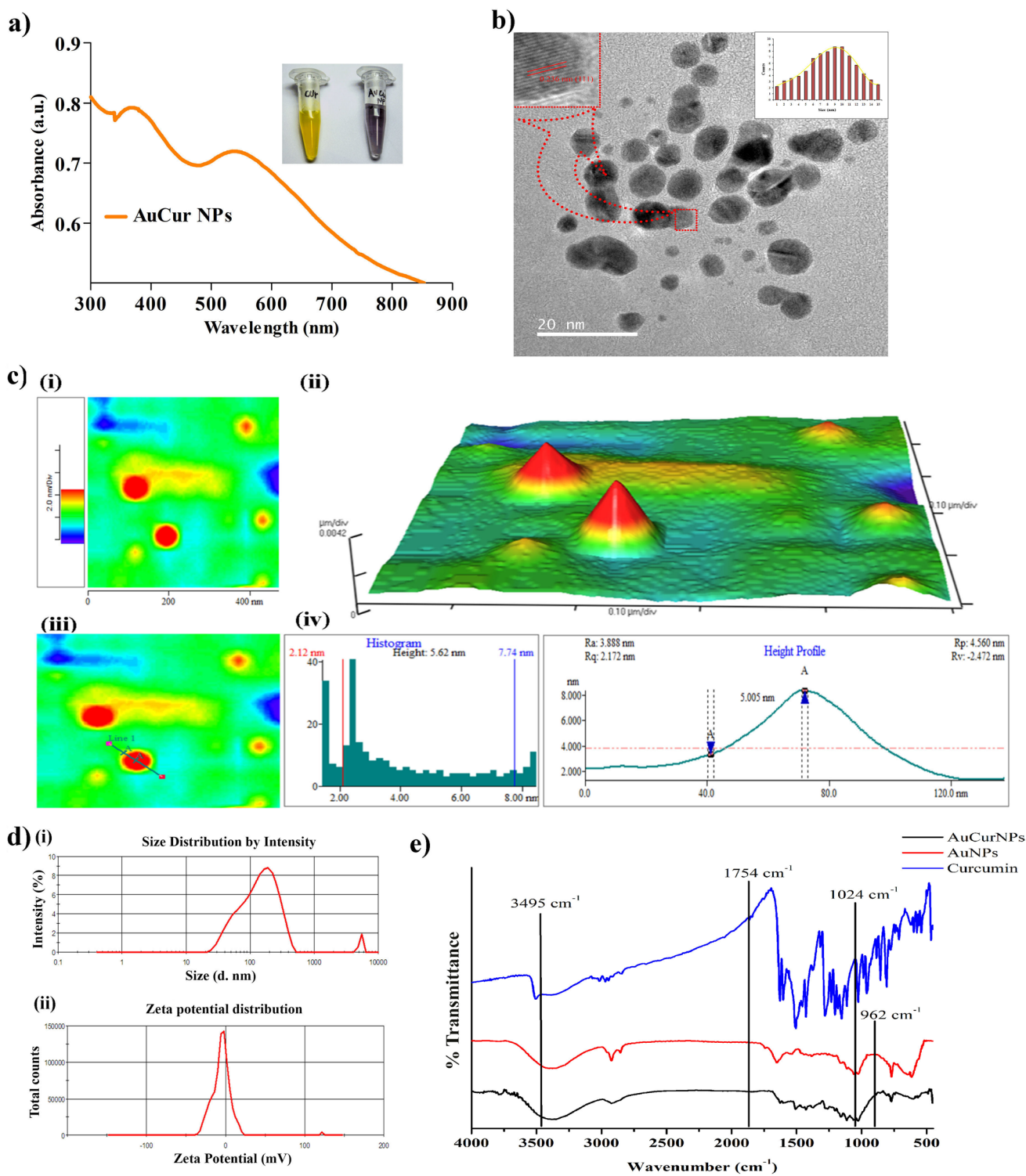


**Fig. 1** Physicochemical characterization of curcumin conjugated gold nanoparticles (AuCur NPs). SPR peak of NPs revealed by **a** UV-visible absorption spectroscopy. Absorbance peak demonstrates the signature peaks for both curcumin and gold in AuCur NPs spectra along with the inset representing the photograph of curcumin and synthesized AuCur NPs; **b** HR-TEM photomicrograph of NPs (inset representing the size distribution pattern of the AuCur NPs); **c** AFM analysis reveals the (i) 2-D view and (ii) represents the 3-D view of AuCur NPs, (iii) and (iv) describing the height profile in term of revealing the size of AuCur NPs; **d** graph revealing the size profiling by particles size analyzer (i) size distribution pattern and (ii) zeta potential measurement; **e** FT-IR spectra of AuCur NPs revealing the conjugation between curcumin and gold nanoparticles

charge of Au ion and the delocalized electron cloud of curcumin acting as a  $\pi$ -donor. This metal–ligand  $\pi$  bonding was also supported by the UV–vis spectroscopic characterization, where the maximum absorbance of curcumin showed a blue shift due to the decrease in the delocalization of electrons, and while a red shift in gold.

The detail of the preparation and physicochemical characterization of AuNPs that describes the particle size and surface morphology was given in previous work [52].

## 2.2 Cell viability and NPs uptake efficiency

The synthesized NPs (AuCur NPs and AuNPs) and curcumin were analyzed for their cytotoxicity activity on HeLa and HEK-293 cells at different concentrations (0–100  $\mu\text{g}/\text{mL}$ ) for 12 and 24 h. The cell viability data of HeLa cells treated with AuCur NPs and curcumin demonstrated a significant reduction in the percentage of viable cells in a dose-dependent and time-dependent manner where the decreasing percentage is more in AuCur NPs as compared to only curcumin-treated cells, which can be attributed to the enhanced bioavailability of curcumin in the nanoparticulated form (Fig. 2a). The cell viability data revealed the  $\text{IC}_{50}$  values were 6.10  $\mu\text{g}/\text{mL}$  and 25  $\mu\text{g}/\text{mL}$  for AuCur NPs and curcumin respectively (Additional file 1: Fig. S2a). On the contrary, the growth pattern and viability of HEK-293 cells were unaffected when incubated with AuCur NPs and curcumin. The results revealed that both AuCur NPs and curcumin treatment groups showed excellent biocompatibility (Fig. 2b). The cell viability studies on cancerous cell line (HeLa) and non-cancerous cell line (HEK-293) describe that curcumin both in free and nanoparticulated form exhibits potent anticancer activity on HeLa cells but remains non-toxic on HEK-293 cells. As proved from previous literature curcumin possesses antioxidant and radioprotection activity [38, 51], and hence this study further estimated its radio-sensitizing and/or radio-protective activities on HeLa and HEK-293 cells respectively. The 50% inhibitory concentration ( $\text{IC}_{50}$ ) doses obtained from HeLa cells were selected and used for subsequent IR-related experiments.

The cell viability data by AuNPs on HEK-293 and HeLa cells also demonstrated insignificantly negligible reduction of both cells (Additional file 1: Fig. S2b and S2c) even at the highest concentration (100  $\mu\text{g}/\text{mL}$ ). In the case of AuNPs, 100  $\mu\text{g}/\text{mL}$  doses were used for radiation-related experiments. The detailed statistical analysis is given in the supplementary information file (Additional file 4: Table S1–S6).

## 2.3 Nanotoxicity assessment in zebrafish

The intriguing biocompatible nature of nanoparticles (AuNPs and AuCur NPs) and curcumin in non-cancerous (HEK-293) cell lines was also validated in the zebrafish embryo. The results demonstrate that the nanoparticles have an insignificant (Additional file 4: Table S7) effect on developing embryos. The embryos showed normal hatching patterns and development of the spine and tail when incubated with AuNPs and AuCur NPs (Additional file 1: Fig. S3). The larvae incubated with AuCur NPs demonstrated the even distribution of NPs as deduced by fluorescence signals throughout the larvae sac as compared to curcumin-treated larvae. Nanoparticulated curcumin had better *in-vivo* bioavailability and distribution as compared to bulk curcumin without any embryotoxicity.

## 2.4 Particle internalization study

For combinational treatment, the doses were selected from the MTT assay but the appropriate time is also a crucial factor for the radiation-involving experiment since the amount of NPs uptake plays a vital function in the enhancement of radiation effects on cells. The uptake of AuCur NPs on HeLa cells at different time points (0–24 h) was quantified by ICP-MS and cellular uptake of curcumin via UV–vis spectroscopy. The metallic content of AuCur NPs taken up by the HeLa cells was elucidated in a time-dependent manner with a steady augmentation in the uptake of AuCur up to 2 h and then significant (Additional file 4: Table S8–S9) amplification in uptake percentage at 12 h (Fig. 2c). Due to impressive photo-physical properties, the uptake of curcumin within cells in free form and nanoparticulated form can be easily surmised through UV–visible absorption spectra. The graph (Fig. 2d) shows the significant enhancement of intracellular curcumin amount released from AuCur NPs into cells. The internalization of AuCur NPs in the HEK-293 cells was also evaluated via ICP-MS and demonstrated in supplementary file 1 (Additional file 1: Fig. S4).

The uptake studies of AuNPs within HeLa cells were also evaluated through ICP-MS and details can be seen in the previously published article [52]. As the understanding of the uptake of nanoparticles within the cells aids in their interaction

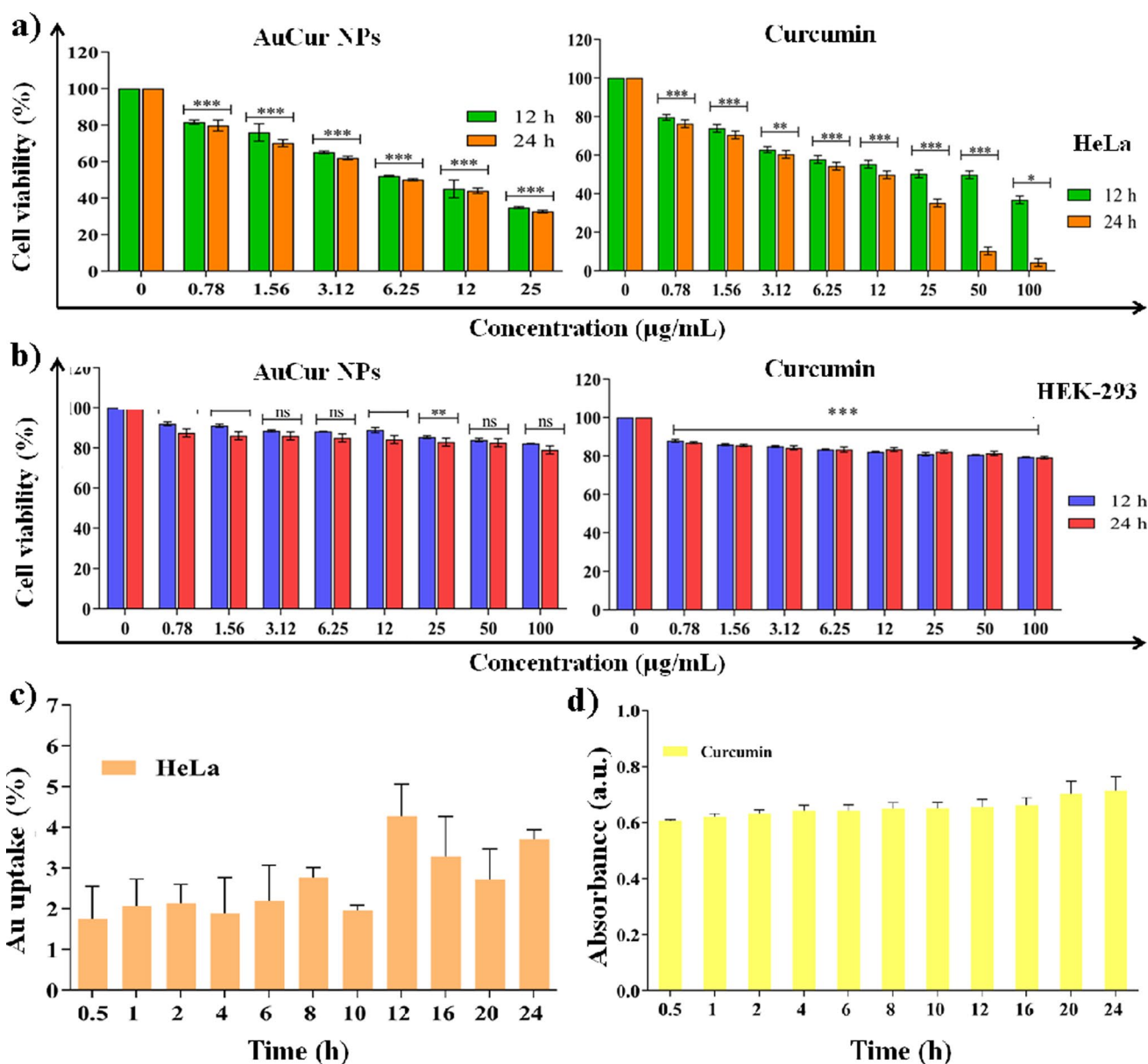


**Fig. 2** Cell viability analysis on cancerous and non-cancerous cell lines. Graph demonstrating the **a** cell viability pattern of HeLa cells; **b** HEK-293 cells treated with curcumin and AuCur NPs at time and dose-dependent pattern evaluated by MTT assay; **c** uptake of AuCur NPs quantified by ICP-MS and **d** curcumin uptake quantified by UV-visible spectroscopy at different time points

and toxicity, thus the selected dose and time for different nanoparticulated systems for further IR dependency study are summarized in Additional file 1: Table S3.

### 2.5 Radio-sensitizing activity of NPs *in-vitro*

HeLa cells were treated with IR in the presence of selected doses of different nanoformulations to monitor the radiation effect on cancer cells. The antiproliferative assay data revealed a decrease in the viability of cells in a dose-dependent manner (2–10 Gy) of IR. The cells irradiated by IR without the pre-incubation of any NPs and/or curcumin showed a reduction in cell viability from 92–60% (at 2–10 Gy). In combined treatment, when cells were pre-incubated with AuCur NPs and then irradiated by IR (AuCur NPs + IR) showed significantly increased mortality of 71–40% at the same IR dose, whereas the curcumin (Curcumin + IR) treated cells showed a slight increase in viability from 83–41% (at 2–10 Gy) in cell population as compare to AuCur NPs + IR group. The cellular population of the AuNPs + IR treated group showed a minor

increase in viability from 86–48% (at 2–10 Gy) as compared to both AuCur NPs and curcumin-treated groups along with IR (Fig. 3a also Additional file 4: Table S10). The number of the viable cell population was higher in the individual treated group as compared to combinational treatment. The cells showed the viability of around 75%, 93%, and 86% for AuCur NPs, AuNPs, and curcumin-treated cells respectively, but a pre-incubation with NPs and/or curcumin followed by IR exhibited potential radiosensitizing effects on HeLa cells.

## 2.6 Clonogenic survival assay

The colony formation assay demonstrates a detailed account of the survival rate and sensitizing enhancement ratio of NPs and/or curcumin in HeLa cells by assessing the number of colonies formed post-radiation treatment. The results demonstrated that the cells pre-incubated with NPs and/or curcumin followed by IR treatment have a significant (Additional file 4: Table S11) reduction in the number of colonies formed as compared to cells irradiated only with IR (2–10 Gy). The

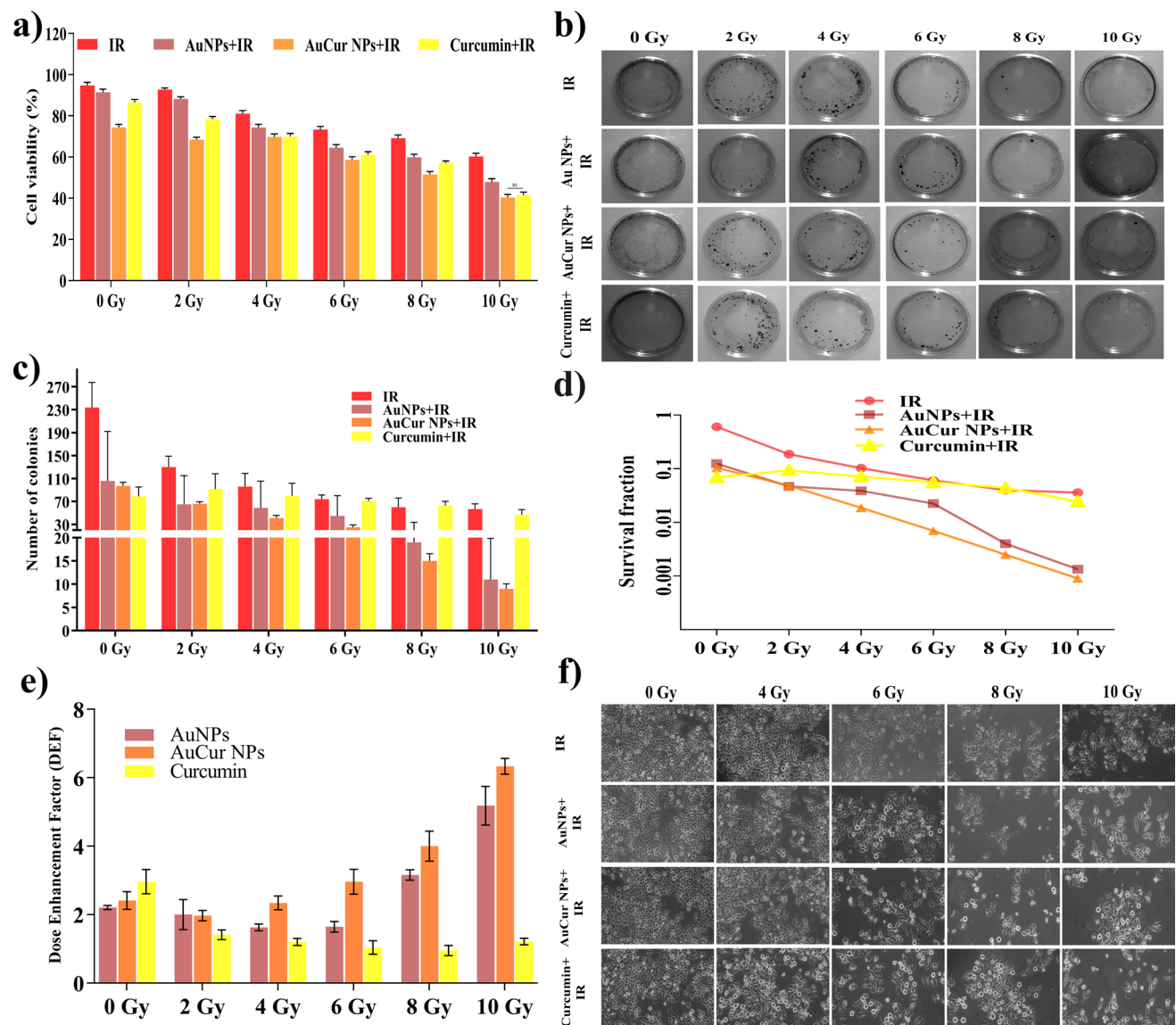


**Fig. 3** Radiosensitizing effect of nanoparticles and/or curcumin. Cell viability pattern of different experimental groups along with and/or without IR on HeLa cells calculated by **a** trypan blue dye exclusion method; **b** photographs of colonies; **c** graph representing the number of corresponding colonies after receiving different treatment; **d** graph demonstrating the survival fraction; **e** graph revealing the sensitization enhancement ratio (SER) after receiving the different treatment; **f** phase-contrast photomicrograph demonstrating the morphological alterations of HeLa cells obtained due to different treatment

photograph and bar plot demonstrate the varying colonies formed (Fig. 3b,c) in the plates in different treatment groups. The cells irradiated by only different doses of IR (2–10 Gy) showed higher *survived* colonies (130–57), but that number decreased in AuCur NPs + IR (66–9), AuNPs + IR (65–11), and curcumin + IR (92–47). The decreased colony-forming pattern indicates the potential of AuCur NPs, AuNPs, and curcumin pre-incubation for radio-sensitization. The clonogenic survival assay for non-cancerous HEK-293 cells demonstrated the number of colonies formed after receiving different doses of IR (Additional file 1: Fig. S5) which is significantly higher in comparison with number of colonies appeared after treatment of HeLa cells.

Cell survival curves, generated from the *linear-quadratic* (LQ) model is a method to describe the relation of radiation dose-dependent cell survivability, used to elaborate on the effect of NPs and curcumin followed by different doses of radiation on cell survival by RAD-ADAPT software (Additional file 1: Fig. S6). The survival curve of the AuCur NPs + IR treated group showed a much steeper gradient line whereas the AuNPs + IR group showed a curved pattern in a gradient line between 2 and 4 Gy but achieved steepness after 6 Gy. Curcumin + IR treated group of cells also showed a slight deviation in the gradient line but steeper than cells treated only with IR. The cells treated only with IR also illustrate a slighter precipitous gradient line as compared to the combinational treatment (Fig. 3d). The survival fraction declines from  $\sim 0.104$  to  $0.0009$  (AuCur NPs + IR group),  $\sim 0.124$  to  $0.001$  (AuNPs + IR), and  $\sim 0.069$  to  $0.024$  (Curcumin + IR) whereas it was about  $\sim 0.608$  to  $0.036$  (IR only) at 0–10 Gy. Thus, the survival fraction data indicates that these combined treatment groups abet the sensitization effect by notably reducing the aptitude of cells to form colonies after different treatments. The  $\alpha$  and  $\beta$  constants estimates of the LQ model and their detailed statistical analysis are given in the supplementary Table (Additional file 1: Table S4 and S5). The detailed statistical analysis is given in the supplementary information file (Additional file 4: Table S12).

The dose enhancement factor (DEF) was also found to be increased in the NPs-treated group (AuCur NPs: 2.96; AuNPs: 1.64 at 6 Gy, respectively) and then the curcumin-treated group (1.04 at 6 Gy). The DEF values divulge that cells treated with NPs have a higher enhancement in dose as compared to curcumin (Fig. 3e). The SER values of NPs and/or curcumin-treated groups with individual IR doses (2–10 Gy) are given in Table (Additional file 1: Table S6). Therefore, this result unveils that the utilization of NPs remarkably enhances the radiosensitivity of HeLa cells by inhibiting cell growth.

## 2.7 Analysis of the synergistic effect of the combination treatment

The analysis using CompuSyn software for synergistic and antagonist patterns at combination treatment (NPs and/or curcumin with IR) revealed that the nanoparticles (AuNPs and AuCur NPs) have strong synergistic behavior at all IR doses (2–10 Gy) as the combination index (CI) is less than 1. While the cells treated with curcumin, along with different radiation doses, are prone to show additive effects in comparison to nanoparticles (the indicative CI values are  $\approx 1$ ). The cells treated with curcumin and 2 Gy radiation dose showed somewhat synergism whereas the cells treated with curcumin and other radiation doses demonstrated the additive effect. The graphical representation of the combination index of nanoparticles and bulk curcumin at different IR doses is given in Additional file 1: Fig. S7. The synergistic pattern is mainly due to an increase in the generation of intracellular ROS within the cells after the interaction of AuNPs and AuCur NPs along with IR. The NPs' interaction with IR results in the release of photoelectric and Auger electrons that further contribute to the production of free radicals. The generation of intracellular ROS due to the production of free radicals is elaborated and explained under ROS generation quantification experiments. The behavior of curcumin under the influence of radiation doses can be attributed to the lower bioavailability of curcumin in its bulk form. Curcumin in its bulk form is prone to get rapidly metabolized and clear out from the cells. Results indicate that the curcumin in nanoparticulated form (AuCur NPs) has a more pronounced activity and bioavailability thereby acting as a potent radiosensitizer and exerting synergistically with IR.

All of the above results corroborate that NPs (AuCur NPs and AuNPs) and/or curcumin have the possibility to act as sensitizers to cancerous cells under the influence of IR. The abilities of these compounds to be exploited as radiosensitizers vary on their surface modification such as curcumin binding on the surface of gold in AuCur NPs that facilitate the release and enhanced bioavailability of curcumin, as well as Au part, engage in the release of secondary photons and electrons of various energy level eventually ionizes the cellular environment and aids in radio-enhancement. The radiosensitizing results indicated that the lowest IR dose (2 Gy) has not demonstrated any significance ( $p < 0.05$ ,  $p < 0.01$ ,  $p < 0.001$ , and  $p < 0.0001$ ) in the sensitization of cells as compared to other doses (Additional file 4: Table S11). Therefore for further experiments, 2 Gy-IR dose was omitted from the sample set for all the individual as well as combinational treatment.



## 2.8 Morphological observations

Further to elucidate the effect of different doses of IR, NPs, and/or curcumin, and their combination (NPs + IR and Curcumin + IR) on cellular morphology, shape, and cell density was monitored by phase-contrast microscopy. The dense morphology, flattened cellular shape, prominent nucleoli, and tight cell-to-cell interaction, cannot be ignored in the case of untreated cells (Fig. 3f). The AuNPs treated cells were revealed to have cellular morphology similar to untreated control whereas those cells treated with AuCur NPs and curcumin demonstrated a comparatively lesser density and shrinkage than untreated control cells.

The combinational treatment with AuCur NPs and IR demonstrated a distorted shape with broken filopodia-like structures, lower cellular density, and cell-to-cell contact. Owing to the higher bioavailability of curcumin in nanoparticulated form *i.e.* AuCur NPs + IR group, the sign of desirable cellular '*health deterioration*' was more prominent in nanoconjugated curcumin than in the Curcumin + IR group. The images of the cells treated with the AuNPs + IR group indicate that the consequential changes in structure, morphology, and density of cells were also in a dose-dependent modus. It was evident from the photomicrographs that during each combinational treatment with IR, the exposed cells seemed to be critically altered and displayed unusual characteristics that included flaccid morphology, inadequacies in adhesion properties to their surfaces, sluggish growth rate, and prominent filopodia-like structures when compared to untreated control cell behaviors.

## 2.9 Reactive oxygen species (ROS) generation

IRs are widely known to raise the intracellular free radicals predominantly ROS by the radiolysis of the water [18]. Normally, the interaction of IR within the cell's microenvironment results in the production of secondary electrons and free radicals which eventually interact with other atoms and produce a chain of biological effects and destabilize the macromolecular structures within cells. Radiosensitizers substantially promote ROS-mediated DNA damages and genomic instabilities by creating nicks in single-strand (SSBs) and/or double-strand breaks (DSBs). The interaction between NPs (AuCur NPs and AuNPs) and incident IR within the cellular microenvironment allows the emission of Auger electrons, potentially harmful at short distances, and enhances the sensitivity of cells for IR by exacerbating ROS generation and eventually DNA damage. The generation of ROS was assessed by fluorescent labeling of cells with H<sub>2</sub>DCFDA dye followed by microscopy. An elevated level of ROS production was displayed by the green fluorescence of DCF, which increases with the increasing doses of IR in all groups (AuCur NPs, AuNPs, and Curcumin) due to the generalized mechanism of ROS generation. Overall results culminate in the synergistic performance of NPs and curcumin in intracellular ROS production than those cells that only receive IR (Fig. 4a). Although it is undeniable that IR plays a crucial role in the elevation of ROS generation and ultimately manifests toxicity to cells by disrupting vital cellular processes. It is not very conclusive from the results of NPs treatment followed by IR treatment which a minimal dose of IR is potentially lethal. Like, the cells pre-incubated with NPs and/or curcumin demonstrated a significantly varying level of ROS when exposed to 6 Gy as compared to unirradiated cells. Thus the cells treated with AuCur NPs + 6 Gy, AuNPs + 6 Gy, and curcumin + 6 Gy overproduce ~9.7, ~7.7, and ~6.8-fold of endogenous ROS (Additional file 1: Fig. S8a and Fig. S8b), respectively, compared with untreated control cells due to the stimulation of enhanced photoelectric free radical production. Therefore, depending on the ROS generation results among all treatment groups, AuCur NPs and AuNPs demonstrate the prospects to be excellent radiosensitizers as compared to bulk curcumin (Additional file 4: Table S12).

## 2.10 DNA fragmentation assay

Damage to the structural integrity of DNA is a hallmark of cell death initiation and ionizing radiation irradiated cells are more prone to DNA damage due to the excess amount of ROS generation. The genomic DNA was isolated from cells that were being exposed to different treatments with and/or without IR and ran on an agarose gel to monitor the alterations in the integrity of DNA. The results portrayed that the untreated control cells display excellent DNA integrity whereas the cells exposed to AuCur NPs + IR revealed fragmented DNA in the form of trails that appeared on the gel. The AuNPs + IR treated group alongside the curcumin + IR group also indicated the breakage of DNA by demonstrating the trailing behavior (Fig. 4b). As it is the well-perceived conception that during programmed cell death laddering phenomenon is usually observed in DNA. It is also to be noted that, the thick band just below the well marked the presence of high molecular

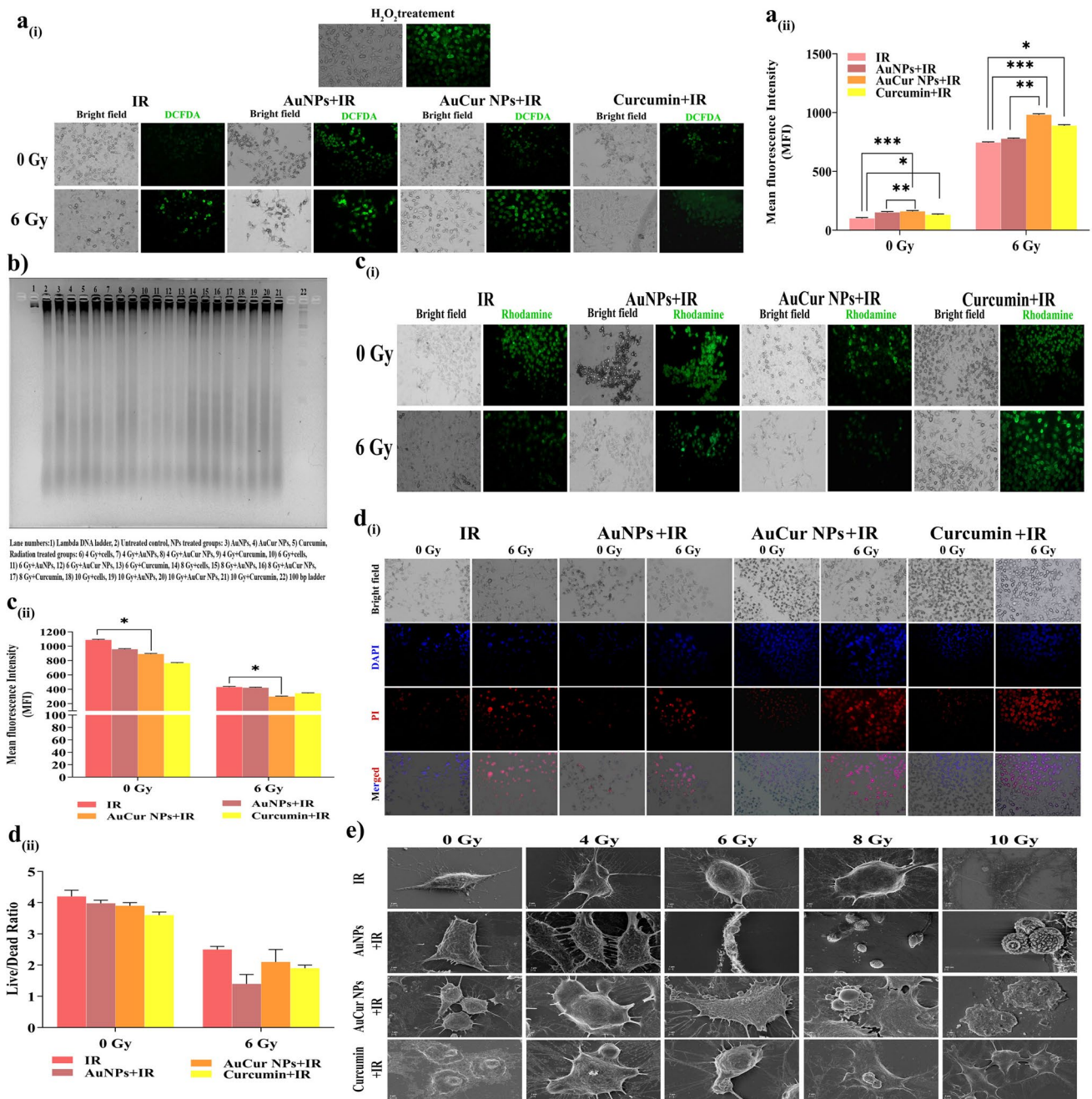


**Fig. 4** Radioenhancement effect of nanoparticles and curcumin in HeLa cells. **a** ROS generation (i) photomicrographs demonstrating the fluorescence signals from the cells, and (ii) corresponding mean fluorescence intensities obtained by DCFDA dye from the cells; **b** genomic DNA fragmentation pattern obtained by giving different treatments; **c** Mitochondrial membrane potential analysis showing (i) fluorescence images of HeLa cells fluorescence intensities obtained by a change in the mitochondrial membrane potential, and (ii) graph showing the corresponding mean fluorescence intensities obtained from the cells; **d** microscopic revelation of (i) apoptotic and non-apoptotic cells stained by DAPI and PI dye and (ii) corresponding mean fluorescence intensities obtained from the cells depicting the ratio of the live-to-dead cell after receiving the different treatments; **e** scanning electron microscopic photomicrograph revealing the morphological alterations, and apoptotic pattern of cells after receiving the different treatments

weight nucleic acids, like genomic DNA. Loss in the thickness of that band indicates more breakage of genomic DNA; in response to the different treatments, the thickness of bands visibly changed indicating different treatment groups have the distinct potential to break the genomic DNA integrity. When cells were pre-incubated with NPs and/or curcumin and then irradiated with different doses of IR, the excessive free radical production further effectuates nicks at various locations and distorts the integrity of DNA, eventually producing ~40–180 bp length intranucleosomal fragments [53, 54].

The data obtained from the LQ model highlights the higher  $\alpha/\beta$  ratio corresponds to a lower capability of repair between the fractions. Hence the effect is due to higher damage production in the presence of NPs system. Also, the effect is not universal, it is dependent on the cell type, the stage of the cell with respect to the cell division, and the size and shape of the particle along with the ligand molecules that are present on the surface of the particle and under the influence of IR can induce oxidative DNA breakage [55, 56]. Therefore, DNA fragmentation results confirmed that synergistic treatment turns out to form a higher amount of oligonucleosomal fragments and hence trailing patterns.

### 2.11 Mitochondrial membrane potential ( $\Delta\psi_m$ ) assay

Mitochondrial functions are considered as the imperative indication of cells' robustness and any dysfunctionality signal towards its faulty behavior. A mitochondrial membrane potential (MMP) assay was performed to monitor any changes in the electrical potential across the inner membranes and its integrity by cationic fluorescent dye (Rhodamine123). The loss in the membrane integrity was monitored by hampered fluorescence intensities of Rhodamine123 dye. Untreated control cells which don't receive any treatment had excellent green fluorescence as compared to cells that were exposed to the different treatment groups. The cells were pre-incubated with NPs and/or curcumin along with 6 Gy demonstrating the significant damage to mitochondrial membrane potential (Fig. 4c). The cells irradiated only with different doses of IR showed depletion in the fluorescence intensities depending on the increasing doses of IR thereby signifying that higher doses are a peril for mitochondrial health. The cells treated with the AuCur NPs + IR group showed inferior fluorescence signals as the IR doses increased which indicates the damage to the inner membranes drastically. The cells treated with the AuNPs + IR group also have low fluorescence intensities depending on the IR doses. The results very conveniently revealed that NPs along with IR initiated the generation of ROS and damaged the membranes of mitochondria and have a characteristic of potent radiosensitizer. The cells treated with the curcumin + IR group also have lower green fluorescence in a dose-dependent manner but the fluorescence intensities were comparatively elevated as compared to the AuCur NPs + IR treated group. Although curcumin in the presence of IR does append in damage to the mitochondrial membrane while its poor bioavailability in a bulk form limits its efficacy (Additional file 1: Fig. S9 and Additional file 4: Table S13).

### 2.12 Apoptotic morphological observations

ROS, DNA fragmentation, and MMP data indicated the nanoformulations have potent radiosensitizer activity that instigates cell death, presumably by apoptosis. To assess the amount of living and dead cells after receiving the respective treatment of NPs, curcumin and/or IR were investigated by co-staining the cells with DAPI/PI dye. These fluorescent dyes aid in distinguishing the cells in different stages of apoptosis *i.e.*, early apoptotic or late apoptotic cells as well as necrotic cells. The microscopic images demonstrated that the PI-stain has exclusively been taken up by dead cells with compromised cellular membrane integrity. Untreated control cells have invariant nuclei staining of DAPI and good morphology whereas the cells exposed to different doses of IR have more strong fluorescent signals of PI-stained cells as the cellular mortality enhanced with an increase in the IR doses (Fig. 4di). The cells treated with the AuCur NPs + IR group have a more diffused DAPI signal due to the presence of fragmented DNA and when these cells were co-stained with PI, the cells exhibit a strong red fluorescence depending on doses of IR. The cells treated with the AuNPs + IR group divulge that the cells showed more PI-stained cells compared to cells irradiated with IR only; the same fluorescent signal pattern is also noticeable in the curcumin + IR treated group. The photomicrographs showed that there are early apoptotic cells stained blue with condensed chromatin whereas late apoptotic cells showed reddish nuclei with comparatively less condensed chromatin. The synergistic therapy was revealed to have elevated ROS, disintegrated DNA, and dysfunctional mitochondrial membrane electric potentiality mediated induced cell death. The data confirmed the stimulation of apoptosis in cells treated with combinational treatment and manifesting a higher death (Fig. 4dii). Therefore, the result indicated that NPs along with IR play a key role in enhancing the doses of IR and inducing apoptosis (Additional file 4: Table S14). The photomicrograph showing the fluorescence signals from cells incubated with different NPs and/or curcumin along with different IR doses (4–10 Gy) is demonstrated in Additional file 1: Fig. S10.

The field emission scanning electron microscopy (FE-SEM) photomicrograph displays the morphologies of cells treated with NPs, curcumin, and/or IR. The cells that undergo apoptosis demonstrated characteristic features such as smaller in size, deformities in their structure, membrane blebbing, and shrunken nuclei. As electron photomicrographs illustrate the untreated control cells showed excellent cellular morphology, whereas the cells exposed to different doses of IR showed changes in the shape, structure, and densities of cells depending on IR doses (Fig. 4e). The cells treated with the combinations of NPs + IR have more rounded cells, lesser cellular densities, shrunken nuclei, membrane blebbing,

and emerging apoptotic bodies. Post-irradiation the growth of the cell diminishes and some cells have to be seen with fragile filopodia-like protruding ends. The results corroborated by the co-staining with DAPI and PI as well as FE-SEM elaborates that the NPs even at lower IR doses significantly sensitized the cells and revealed prominent apoptotic features as compared to cells exposed to only IR even at higher doses.

### 2.13 Cell cycle analysis

To pinpoint the role of NPs and/or curcumin along with IR dose, cell cycle regulation was analyzed to validate the cell cycle blockade pattern. Interestingly, DNA histogram-based estimation of cell distribution in different stages of the cell cycle indicates radiation-induced sensitivity contributed to disruption in normal cell cycle regulation. The cell cycle data demonstrated that the cells, that received different treatments of NPs and/or curcumin along with IR, were mainly arrested at the  $G_0$ - $G_1$  phase. The cells arrested at sub- $G_0$ - $G_1$  typically correspond to apoptotic populations. The apoptotic cell populations were found to be more in the AuCur + IR group (~12.30%) and AuNPs + IR group (~10%) as compared to the curcumin + IR group (~4.18%). The graph reveals the percentage of cells at all stages of the cell cycle when pre-incubated with NPs and/or curcumin and then irradiated with a 6 Gy dose (Fig. 5a). The complete set of results indicated that untreated control cells were distributed *naturally* at all stages of the cell cycle. The comprehensive representation of the cell population at different cell cycle stages after combinational treatment and/or individual treatment with all different IR doses is given in Additional file 1: Fig. S11.

ROS, analysis of mitochondrial membrane potential, investigation of cell death, and cell cycle results indicated that IR dose (4 Gy) has a lower level of significance ( $p < 0.05$ ) even in the presence of NPs and/or curcumin. The data revealed that the higher doses have more significance ( $p < 0.01$ ,  $p < 0.001$ , and  $p < 0.0001$ ) Therefore, for further experiments 4 Gy IR dose was omitted for all the individual and combinational treatments.

### 2.14 Wound healing assay

The cytoskeleton outlines the infrastructure for cell shape and additionally contributes to cell motility. Cell migration has a remarkable role in embryonic development, angiogenesis, and tumor metastasis. Cell-to-cell interaction is a significant factor for the survival of cells under stress conditions like during and after radiation exposures. In cell migration assay, the cells are forced to move in one direction, via cell-to-cell contact, and evaluated its innate ability for directional persistence. To further confirm the sensitizing capabilities of NPs and/or curcumin on HeLa cells; the wound-healing assay or scratch assay was performed on the monolayer of cells. The role of an excellent radiosensitizer tends to hamper the migration abilities of cells. The results elucidated untreated control cells have several membrane protrusions and showed higher cellular migration at 48 h whereas the cells that received different treatments (NPs and/or curcumin) along with different doses of IR (6–10 Gy) were prone to have significantly repressed functional filopodia formation and depletion in migration abilities eventually inclined towards incompetence to heal the created 'wounds' (Fig. 5b). Data concluded that the cellular motility was inhibited upon the pre-incubation of NPs and/or curcumin even if monitored for 48 h, with significantly higher efficiency than only radiation treatment. The wound in the form of a gap (distance) was quantitatively evaluated by ImageJ software. The significant reduction in the filopodia protrusions also makes cancerous cells incapable of 'metastasis' and the application of NPs supplies better assistance to radiations and manifests them to be an enviable radiosensitizer. The effect of NPs and/or curcumin along with different doses of radiation (6–8 Gy) is given in Additional file 1: Fig. S12 and significance values in Additional file 4: Table S15.

### 2.15 Validation of experimental data by random response surface methodology

Evaluation of designed experiments is crucial for estimating the role of effectors and their consequent effects. It becomes complex when various effectors and their effects need to be validated to determine the ultimate fate of experimentations. It is also notable that determining the most effective solution becomes a paradox when effects are not distinguishably different in the presence of complex and/or compound effectors. Hence, a *reverse experiment design* approach was adopted to determine the most effective combination of treatments, *i.e.*, NPs and/or curcumin along with different doses of IR. As it has been proved that IR doses (2 and 4 Gy) didn't show any significant effect on cells either in individual or combinational treatment. Hence, to determine the puissant combination among the pairs, three IR doses (6, 8, and 10 Gy) with NPs and/or curcumin were estimated by a modified randomized reduced quadratic *Response Surface Design* (RSM) method in Design-Expert® software. For this mathematical and statistical experimentation method, different treatments were

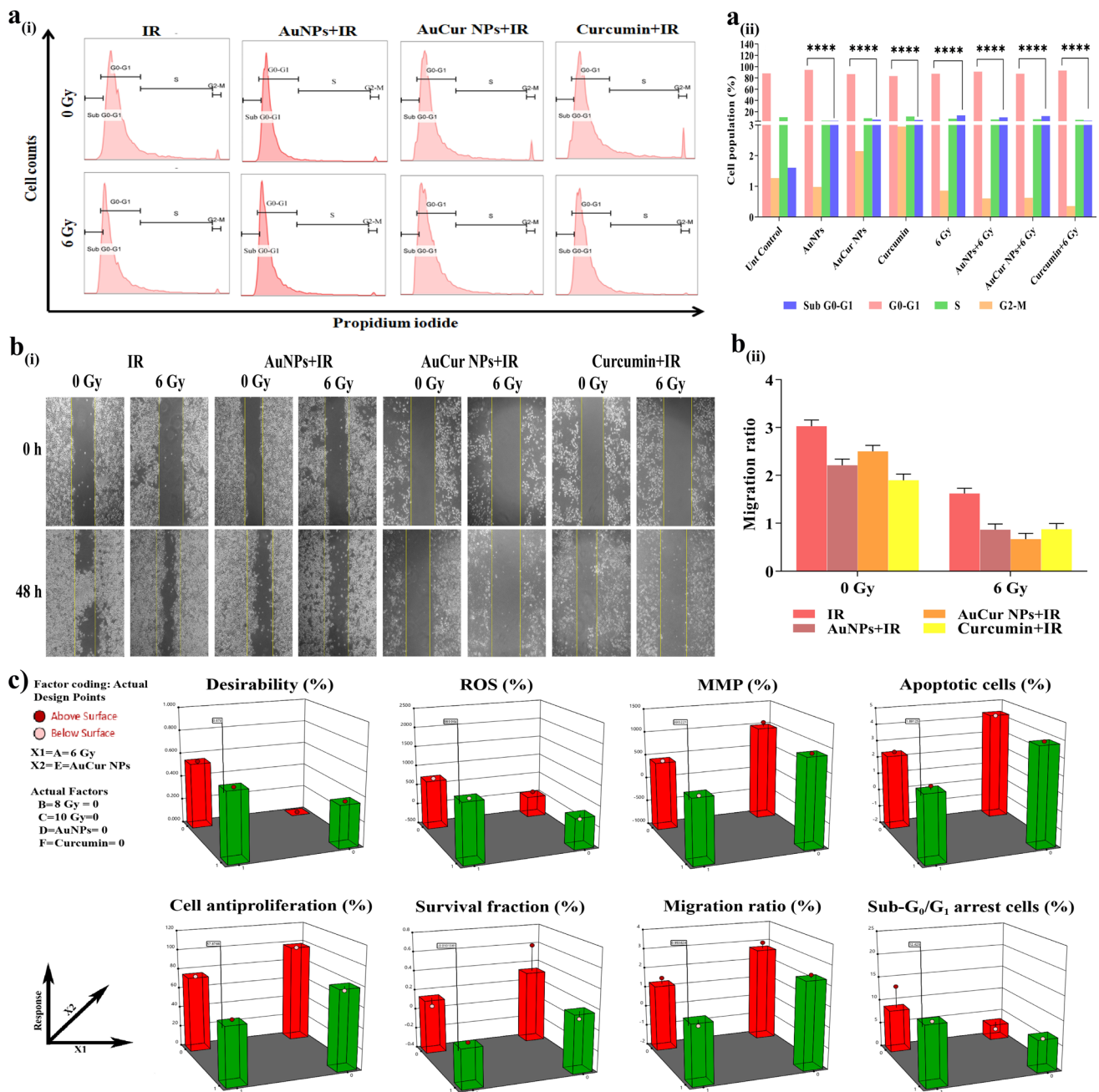


**Fig. 5** Radioenhancement effect of nanoparticles and/or curcumin. **a** Cell cycle analysis (i) cell population arrest peaks of treated and untreated HeLa cells and (ii) graph showing the cell cycle arrest percentage at different stages of cell cycle regulations; **b** scratch assay (i) microscopic images showing the migration abilities of HeLa cells after receiving the different treatments and (ii) graph representing the migration ratio of cells; **c** graph showing the three dimensional (3D) representation of obtained responses for individual experiments in significant dose (6 Gy) and NPs combination (AuCur NPs) by response surface design

considered as variable factors (IR doses, AuNPs, AuCur NPs, and curcumin) and dependent responses were cell percentage of different experiments (*i.e.*, ROS generation, mitochondrial membrane potential analysis, cell death, the antiproliferative population of cells, survival fraction, migration ratio, and cell cycle). The RSM analysis data showed intriguing observation that the most desired output which was statistically significant was the combination of AuCur NPs along with IR dose (6 Gy) among all other combinations in a more effective way on HeLa cells (Fig. 5c). The detailed statistical analysis of ANOVA for the sequential method, the correlation coefficient of coded factors, generated polynomial equations, and confirmation of post-analysis are given in supplementary information (Additional file 1: Table S7–S11). All the key radiosensitization experiments demonstrate the enhancement in the therapeutic index by using curcumin-conjugated gold

nanoparticles but curcumin also has radioprotection abilities, depending on the cellular microenvironment, favorable in non-cancerous cells. The evaluation of radioprotection abilities of bulk curcumin and nanoparticle conjugated curcumin showed a promising difference in quenching the intracellular free radicals and neutralizing the redox environment by nanoconjugated curcumin as compared to bulk curcumin in HEK-293 cells (Additional file 1: Fig. S13), this can be attributed to the difference of biologically available curcumin in nanoconjugated and bulk forms.

## 2.16 Quantitative real-time PCR assay

The quantitative reverse transcription PCR (qRT-PCR) method very efficiently demonstrates the precise and insightful alterations in the gene expression pattern. To identify the role of NPs and/or curcumin individually or along with IR on cell death mechanisms, some crucial program cell death (PCD) related genes were analyzed through the qRT-PCR technique. qRT-PCR (PCR) for a selected set of genes indicates that radiation treatment alone or with a combination of radiosensitizer molecules has an intense effect on the transcriptional level expression of these genes. *c-MYC*, a proto-oncogene, and a crucial transcription factor is associated with several intracellular processes at the molecular level with a disproportionately high expression in several cancer types [57, 58]. *TP53*, *CYCS*, *BAX*, and *CASP3* act as apoptotic genes and participate at different stages of the apoptosis mechanism. During the apoptotic process, these genes participated in apoptosis initiation (*TP53*), progression (*CYCS*), and execution (*CASP3* and *BAX*).

The *c-Myc* gene product plays a pivotal role in cellular proliferation and thereby contributes to the formation of cancer. The constitutive upregulation of this proto-oncogene (*c-Myc* gene) is mainly found in the different cancer subtypes including cervical cancer, breast cancer, colon cancer, and stomach cancer [58]. Several studies demonstrated the effect association between radiosensitivity and deregulated *c-Myc* [59–61]. Other studies also indicated that an uncontrolled upregulation of the *c-MYC* gene enhances cell apoptosis stimuli in the radio-sensitized cells to significantly facilitate apoptosis [61, 62]. The balance between deregulated *MYC* and other apoptotic genes *i.e.* *TP53*, *CASP3*, *CYCS*, and *BAX* is crucial in triggering the PCD process in cancerous cells. *MYC* gene upregulation manifested in IR-treated groups predominantly plays a critical role in triggering the *CYCS* gene in apoptosis-mediated pathways by releasing it in the cytoplasm [62]. Released *CYCS* in cytoplasm work in association with other components of programmed cell death machinery. Moreover, upregulation of the *BAX* level is equally critical to induce the opening of a voltage-dependent anion channel (VDAC) that triggers the release of *CYCS*. The release of *CYCS* from mitochondrial membranes into cytoplasm induces the formation of apoptosomes in the presence of apoptotic protease activating factor-1 (Apaf-1) thereby activating the pro-caspase-9. The expression data revealed that in the cells treated with NPs and/or curcumin along with different doses of IR, the *BAX* expression is relatively low except for the 6 Gy radiation dose.

Ionizing radiations are known to generate double-strand-DNA (ds-DNA) nicks and breakage into smaller oligomers. Due to the exposure of IR on cells, several ds-DNA nicks were observed that further activate the Interferon-inducible protein (AIM-2). AIM-2 is a cytoplasmic sensor molecule that non-specifically recognizes ~ 40 bp long ds-DNA nicks and activates the apoptosis-associated speck-like protein containing a CARD (ASC). Activated ASC is responsible for caspase-1 binding and formation of AIM-2 inflammasome which further initiates the activation of pro-inflammatory cytokines thereby inducing pyroptosis. During the pyroptosis, the elevated expression of *BAX*, *CASP-3*, *CASP-9*, and *TP53* was observed along with other genes. The results demonstrated that the AuNPs are biocompatible in nature and unlikely to have any significant role in the up-and/or down-regulation of the genes when given to cells. On the contrary, curcumin is known as a direct blocker of dual-specificity tyrosine-regulated kinase-2 (DYRK2) which further activates the series of proteasomes [63, 64]. Further, curcumin-conjugated AuNPs potentially trigger the TP53-mediated apoptosis via activating the caspase-3 pathway. The results demonstrate a significant ( $p < 0.05$ ) up-regulation in the *MYC* (~ 7.86 fold), *TP53* (~ 6.19 fold), *CASP-3* (~ 3.86 fold), and *CYCS* (~ 7.69 fold), *BAX* (~ 4.12 fold) in the IR (6 Gy) group were observed. On the contrary, there was a most significant upregulation of gene *MYC* (~ 7.15 fold), *TP53* (~ 7.14 fold), *CASP-3* (~ 9.90 fold), and *CYCS* (~ 10.80 fold), *BAX* (~ 10.33 fold) in the AuCur + 6 Gy group. This upregulation pattern is not noticeable in only the curcumin treatment group due to the lower bioavailability of the bulk curcumin. Thus, the results demonstrated that under the influence of IR, all treatment groups (NPs and/or curcumin) have a more pronounced result as compared to individual treatment, and *visa-versa*.

In the case of nanoformulations, the incidence of ionizing radiation interacts with nanoformulations and generates oscillating Auger electrons to facilitate the release of conjugated curcumin from the surface of AuCur NPs into the cells. The released curcumin initiates the cascade of cell death in cancerous cells. Under the influence of IRs, the AuNPs pre-incubated cells, the photoelectric effect occurs that eventually generates the localized heat and free radicals within cells thereby initiating the breakdown of genomic DNA into smaller oligomeric fragments. Therefore, the generation of

localized heat and free radicals within cells initiates two pathways in particular namely apoptosis and pyroptosis. The most significant change in the expression of *BAX* gene expression revealed that the upregulations were observed more in AuCur NPs + 6 Gy (~ 10.33 fold), AuNPs + 6 Gy (~ 8.26 fold), curcumin + 6 Gy (~ 6.41 fold) and 6 Gy (~ 4.12 fold) respectively, indicating noteworthy transcriptional changes in the cells exposed to 6 Gy IR dose along with the combination of particles (Fig. 6a). The interaction of cells with ionizing radiation usually promotes the development of irreparable DNA damages that further contribute to genomic instability, oxidative stress, and the initiation of apoptosis-mediated cell death. The DNA damage caused due to IR leads to the accumulation of p53 stimuli that act as modulators for pro-apoptotic effectors. Therefore, the results demonstrated that in NPs and/or curcumin-sensitized cells at higher doses of IR *i.e.* 8 Gy and 10 Gy, mislaying the intricate balance of mentioned gene products thereby had an ineffective role in triggering c-Myc-dependent blocking. While the cells receive only a high dose of IR revealed to be evidence for significant participation in c-Myc-dependent apoptosis. Therefore, gene expression data confirmed that AuCur NPs alone may not initiate the apoptosis mechanism but are evidently triggered in the presence of ionizing radiation. The observations indicated that combinational treatment (NPs and/or curcumin) along with ionizing radiation facilitated the more pronounced effect even at a lower IR dose (6 Gy) thereby enhancing the therapeutic index IR and can be used for better radiotherapeutic therapy.

Further, the results attained from gene expression data, after hierarchical clustering based on the Ward linkage from Pearson correlation coefficients, indicate (Fig. 6b) that the effect of different types of treatment has a very distinct overall effect on the expression of these genes and constructed by using Orange software [65]. It is very interesting to see that the highest dose, *i.e.*, 10 Gy clustered under the same clade as the untreated control, which indicates the incompetency of the specific radiation dose when compared with the tested classes of genes. On the other hand, all 6 Gy treatments, except AuNPs + 6 Gy which also appear to be another *closest relative* of untreated control, come under a single clade as an indicative of the most consistent group of treatment.

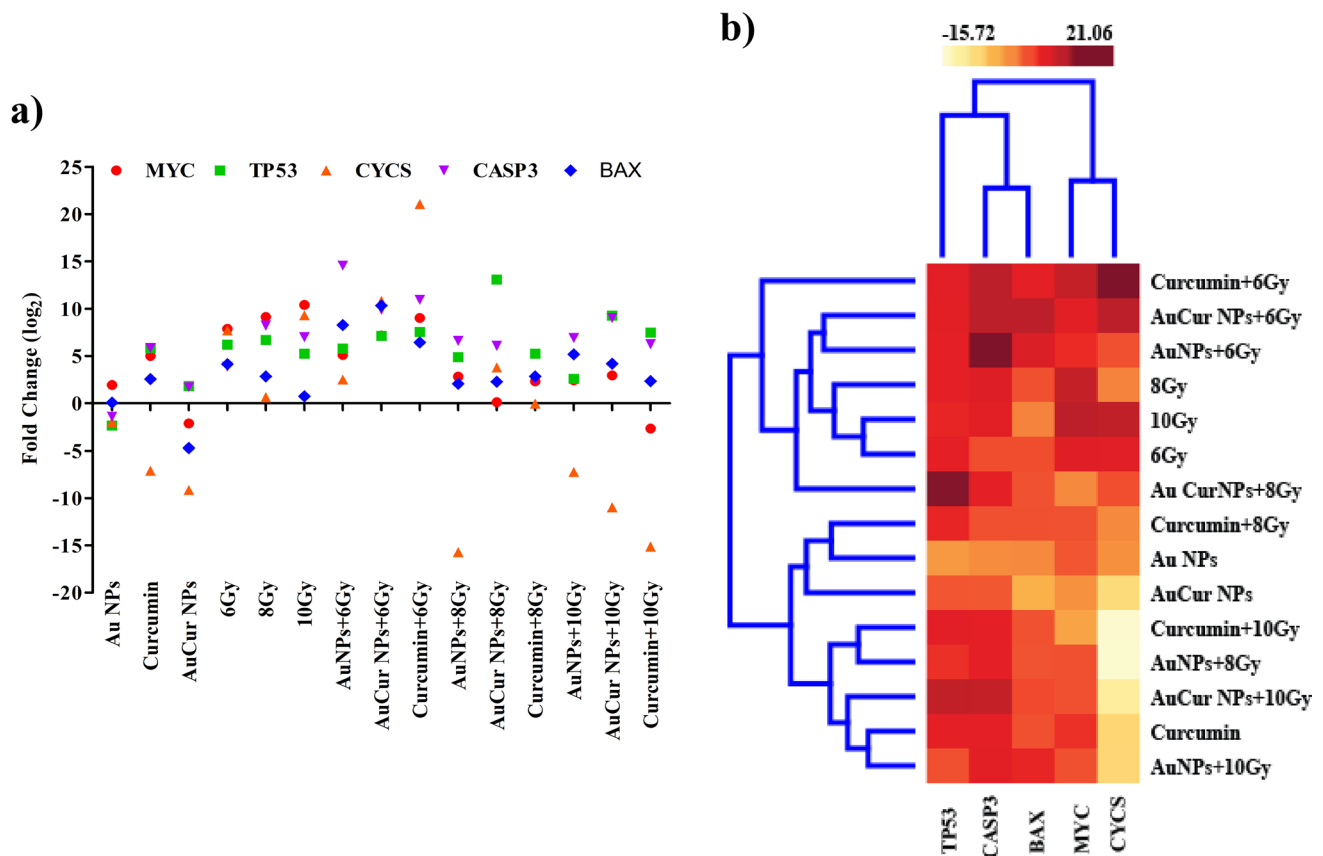


**Fig. 6** Quantitative real-time PCR analysis. **a** graph showing the fold change expression pattern of different genes in HeLa cells after receiving the different treatments, and **b** image demonstrating the heat-map and cluster relationship between the different genes and experimental groups

## 2.17 Molecular mechanism of the signaling pathway

The confusing yet interesting pattern of gene expression change leads to the identification of the probable molecular pathway of the action. For this analysis, only the best combination *i.e.*, AuCur NP + 6 Gy considered to construct the probable mechanism of action at the molecular level. Curated databases such as STRING database and KEGG database were used to analyze pathway network that provides comprehensive genome-wide networks that include whole gene regulations, signal transduction, and gene protein associations. For this study, a confidence-based full-scale STRING network [66] was built by keeping the interaction score at the highest confidence level (0.900) with a maximum of 50 interactors at the first shell. Thus, the build protein–protein interaction (PPI) network has a very high overall enrichment value ( $< 1.0e^{-16}$ ) signifying a large number of possible interactions, which is also validated by the number of edges present between nodes. The final number of nodes are 55 (50 + original 5 query proteins) and the corresponding edge number is 228 (Fig. 7a). Most of the interactions indicate different biological processes related to several environmental effectors, diseased conditions, and others, along with several local network clusters; given in the supplementary information files (Additional files 2, 3). Further, in this study the components from two biological processes related to gamma radiation's effect on cells, *viz.* GO: 0071480 (blue dot) and GO: 0010332 (red dot) along with two local network clusters of STRING, CL: 18,767 (yellow dot) related to the *Activation of caspases through apoptosome-mediated cleavage* and CL: 18,741 (green dot) correspond to *Nanomaterial induced apoptosis, and TRAIL binding* (Fig. 7b) was selected for further analysis in KEGG database [67, 68]. KEGG Mapper Reconstruct analysis on selected 11 proteins (including originally analyzed five genes by gene expression study) reveals 104 pathways are associated with the examined proteins. Among all of them, apoptosis (map. 04210), p53 signaling pathway (map. 04115), and cellular senescence (map. 04218) along with an external candidate map cytosolic DNA sensing pathway (map. 04623) considered based on the experimental procedure and results obtained, to reconstruct the predictive mechanism pathway.

The predictive pathways explained that the gene products indicate the involvement of programmed cell death (PCD). During PCD, the initial signals are generated via damage of DNA followed by activation of caspases in response to anticancer chemotherapy and/or radiation therapy thereby initiating the extrinsic pathway or at the mitochondria by stimulating the intrinsic pathway. Figure 7c illustrates the comprehensive predictive pathway for the functioning of nanomaterials along with ionizing radiation by using the KEGG mapper. Ionizing radiations mediated single and double-strand breaks in nuclear DNA eventually activate the caspases. These caspases cleave several substrates in the cytoplasm or nucleus leading to many of the morphological features of apoptotic cell death. During apoptosis, polynucleosomal DNA fragmentation is mediated by the cleavage of an inhibitor of caspase-activated DNase that cleaves the DNA further into oligomeric fragmentations. The mitochondrial pathway is initiated by the release of cytochrome c into cytosol which further triggers caspase-3 activation. Caspase activation is also linked to the permeabilization of the outer mitochondrial membrane due to stress signals. The oxidative stress (ROS) induced changes in the apoptotic signals to cells exposed to NPs and/or curcumin along with IR were conveyed by significant alterations in the mRNA expressions by up- and downstream signaling pathways involved in apoptosis and injury in cells. Therefore, from the experimental evidence and the previous work, pathway reconstruction certainly indicates that the mechanism of cell killing by combinational treatment affects cellular components in three distinct ways, *i.e.*, apoptosis, pyroptosis, and cell cycle arrest. Though, some of the interactions are still unknown but can be elucidated by experimental procedures.

## 3 Conclusion

Ionizing radiation, in the form of an external beam or as internal medicine, has become a vital part of modern cancer therapy as well as diagnostic purposes. Radiotherapy is the most widespread method used in cancer patients to shrink the tumor or eradicate residual tumor cells but unfortunately, increased radiation exposure is associated with radiation-related adverse events which include single and double-strand DNA damages and deficiencies in DNA repair mechanisms, at a molecular level. There was enhanced intracellular ROS generation due to secondary effects of the IR and these reactive species are quick enough to oxidize macromolecules (*i.e.*, DNA, proteins, and lipids) present within the cells which ultimately leads to the induction of cell death and mitotic failure. Cells having a higher



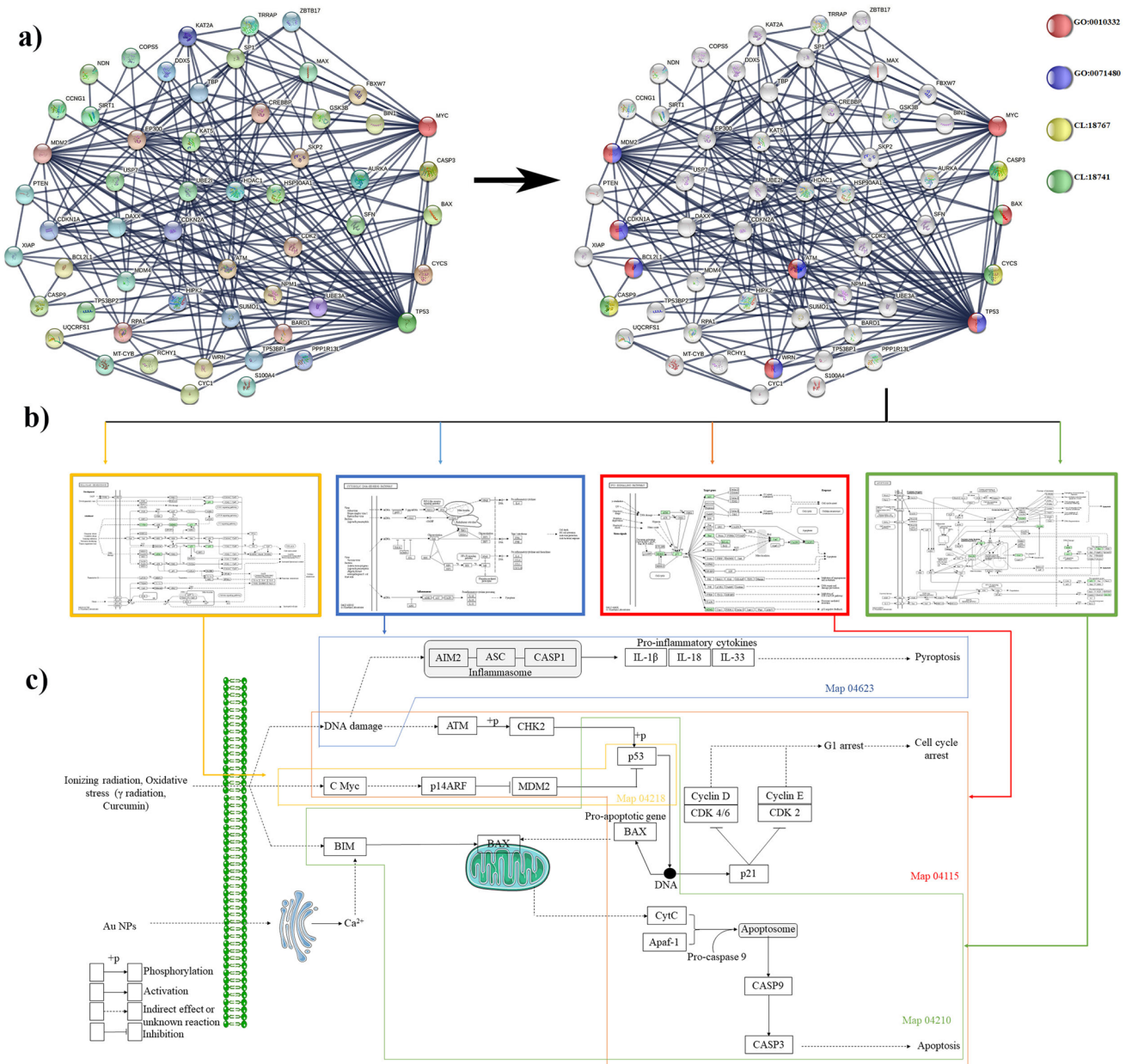


**Fig. 7** Interaction between Genes and retrieval of molecular pathways. **a** STRING protein–protein interaction pathway analysis. The image shows the cluster-based interrelation between the identified genes (*MYC*, *TP53*, *CASP3*, *CYCS*, and *BAX*) and biological processes; **b** probable interaction pathways such as apoptosis (map. 04210), p53 signaling pathway (map. 04115), and cellular senescence (map. 04218) along with an external candidate map cytosolic DNA sensing pathway (map. 04623) was considered to reconstruct the predictive pathway for radio-enhancement of nanoparticles; **c** comprehensive representation of predictive pathway for the functioning of nanomaterials along with ionizing radiation by using KEGG mapper

proliferation rate are more sensitive to IR as compared to quiescent and/or slowly dividing cells. IR strikes tumors as well as inevitably reaches healthy cells imprecisely to incorporate chromosomal abnormalities which further enhance the chances of new malignancies. In conclusion, this report significantly highlights the comparison between bulk curcumin and nanoparticulated curcumin in a gold-conjugated form for its radio-enhancement abilities. This study has successfully exploited the gamma radiation’s total cross-sectional effect with the presence of gold nanoparticles’ intrinsic photoelectric effect, along with curcumin’s pH-dependent isomerization for the initiation of a violent chain of intracellular reactions due to the outburst of highly reactive intermediates. Hence, it is obvious to observe the conspicuous presence of the gold-curcumin combination during radiation treatment. Biologically available curcumin tends to elevate the generation of intracellular ROS levels and also induces significant IR-mediated mitochondrial

membrane loss leading to the apoptosis of cancer cells. Genome instability and enhanced apoptosis are the critical signatures of radiation-induced changes in cells. The cell cycle analysis, apoptotic signals, and DNA damage were monitored in cells additionally an increased transcriptional up-regulation in gene products (*c-Myc*, *TP53*, *CYCS*, *CASP-3*, and *BAX*). Our finding demonstrates that HeLa cells preexposed to AuCur NPs have elevated apoptotic and pyroptotic signaling than only radiation-exposed cells. This radiosensitizing effect of AuCur NPs is not only proved by the experimental method but also well supported by statistical modeling. Along with that the nanoparticulated curcumin also exhibits participation in prolonged radical scavenging in normal cells. Though the data are limited but it appreciably demonstrates radiation protection on HEK-293 cells when exposed to gamma radiation in the presence of AuCur NPs. This study again paved the path for the search for a single combination-dependent radio modulator, which can easily enhance the radiation effect in cancer cells along with giving protection to normal cells.

## 4 Experimental section

The full experimental section is provided in the Supplemental information file 1 (SI).

**Acknowledgements** The authors would like to express their earnest gratitude to Dr. Sayan Bhattacharya for providing his lab fluorescence microscopy and other facilities at the Department of Chemical Sciences, IISER-Kolkata, West Bengal, India.

**Author contributions** P.Y., A.B., and K.S. conceptualized the study. P.Y. and A.B. designed and performed the methodology. P.Y. and A.B. analyzed and visualized the data and performed a formal analysis. P.Y. and A.B. wrote the main manuscript and review, edit the original draft. All authors reviewed the manuscript.

**Funding** Priya Yadav is thankful to the Indian Council for medical research, the government of India for the Senior Research Fellowship (ICMR-SRF; No.: 45/30/2018-NAN/BMS), and Arghya Bandyopadhyay is thankful to the Science and Engineering Research Board under Department of Science and Technology (SERB-DST), the Government of India for the National Postdoctoral Fellowship (SERB-NPDF, No.: PDF/2018/001043). The authors are also thankful to the DST-Nanomission scheme (SR/NM/NS-1447/2014), Government of India for financial support.

**Data availability** The authors confirm that the data supporting the findings of this study are available within the article and its supplementary materials.

## Declarations

**Competing interests** The authors declare no competing interests.

**Open Access** This article is licensed under a Creative Commons Attribution-NonCommercial-NoDerivatives 4.0 International License, which permits any non-commercial use, sharing, distribution and reproduction in any medium or format, as long as you give appropriate credit to the original author(s) and the source, provide a link to the Creative Commons licence, and indicate if you modified the licensed material. You do not have permission under this licence to share adapted material derived from this article or parts of it. The images or other third party material in this article are included in the article's Creative Commons licence, unless indicated otherwise in a credit line to the material. If material is not included in the article's Creative Commons licence and your intended use is not permitted by statutory regulation or exceeds the permitted use, you will need to obtain permission directly from the copyright holder. To view a copy of this licence, visit <http://creativecommons.org/licenses/by-nc-nd/4.0/>.

## References

1. Zhang Z, Liu X, Chen D, Yu J. Radiotherapy combined with immunotherapy: the dawn of cancer treatment. *Signal Transduct Target Ther.* 2022;7:258.
2. Ostuni E, Taylor MRG. Commercial and business aspects of alpha radioligand therapeutics. *Front Med.* 2023;9:1070497.
3. Jadvar H. Targeted radionuclide therapy: an evolution toward precision cancer treatment. *Am J Roentgenol.* 2017;209:277–88.
4. Yeong C-H, Cheng M-h, Ng K-H: Therapeutic radionuclides in nuclear medicine: current and future prospects. *J Zhejiang Univ Sci B.* 2014;15:845–63.
5. Sgouros G, Bodei L, McDevitt MR, Nedrow JR. Radiopharmaceutical therapy in cancer: clinical advances and challenges. *Nat Rev Drug Discovery.* 2020;19:589–608.
6. Ku A, Facca VJ, Cai Z, Reilly RM. Auger electrons for cancer therapy: a review. *EJNMMI Radiopharm Chem.* 2019;4:27.
7. Onoue R, Watanabe H, Ono M. Hoechst-tagged radioiodinated BODIPY derivative for Auger-electron cancer therapy. *Chem Commun.* 2023;59:928–31.
8. Falzone N, Cornelissen B, Vallis KA. Auger Emitting radiopharmaceuticals for cancer therapy. In: García Gómez-Tejedor G, Fuss MC, editors. *Radiation damage in biomolecular systems.* Dordrecht: Springer; 2012. p. 461–78.

9. Idrissou MB, Pichard A, Tee B, Kibedi T, Poty S, Pouget J-P. Targeted radionuclide therapy using auger electron emitters: the quest for the right vector and the right radionuclide. *Pharmaceutics*. 2021;13:980.
10. Choi J, Kim G, Cho SB, Im H-J. Radiosensitizing high-Z metal nanoparticles for enhanced radiotherapy of glioblastoma multiforme. *J Nanobiotechnol*. 2020;18:122.
11. Dasari S, Bernard Tchounwou P. Cisplatin in cancer therapy: molecular mechanisms of action. *Eur J Pharmacol*. 2014;740:364–78.
12. Townsend DM, Deng M, Zhang L, Lapus MG, Hanigan MH. Metabolism of cisplatin to a nephrotoxin in proximal tubule cells. *J Am Soc Nephrol*. 2003;14:1.
13. Farooq MU, Novosad V, Rozhkova EA, Wali H, Ali A, Fateh AA, Neogi PB, Neogi A, Wang Z. Gold nanoparticles-enabled efficient dual delivery of anticancer therapeutics to hela cells. *Sci Rep*. 2018;8:2907.
14. Zheng F, Wang P, Du Q, Chen Y, Liu N. Simultaneous and ultrasensitive detection of foodborne bacteria by gold nanoparticles-amplified microcantilever array biosensor. *Front Chem*. 2019;7:232.
15. Janic B, Brown SL, Liu F, Mao G, Chetty IJ, Movsas B, Wen N. Gold nanoparticles as radiosensitizers in MDA MB 231 xenograft mouse model. *Int J Radiat Oncol Biol Phys*. 2019;105:E677–8.
16. Torres-González L, Díaz-Ayala R, Vega-Olivencia CA, López-Garriga J. Characterization of recombinant his-tag protein immobilized onto functionalized gold nanoparticles. *Sensors (Basel, Switzerland)*. 2018;18:4262.
17. García Calavia P, Bruce G, Pérez-García L, Russell DA. Photosensitizer-gold nanoparticle conjugates for photodynamic therapy of cancer. *Photochem Photobiol Sci*. 2018;17:1534–52.
18. Kaur P, Aliru ML, Chadha AS, Asea A, Krishnan S. Hyperthermia using nanoparticles—Promises and pitfalls. *Int J Hyperthermia Off J Eur Soc Hyperthermic Oncol North Am Hyperthermia Group*. 2016;32:76–88.
19. Goswami N, Luo Z, Yuan X, Leong DT, Xie J. Engineering gold-based radiosensitizers for cancer radiotherapy. *Mater Horiz*. 2017;4:817–31.
20. Choi BJ, Jung KO, Graves EE, Pratz G. A gold nanoparticle system for the enhancement of radiotherapy and simultaneous monitoring of reactive-oxygen-species formation. *Nanotechnology*. 2018;29: 504001.
21. Sevilla MD, Becker D, Kumar A, Adhikary A. Gamma and ion-beam irradiation of DNA: free radical mechanisms, electron effects, and radiation chemical track structure. *Radiat Phys Chem*. 2016;128:60–74.
22. Reisz JA, Bansal N, Qian J, Zhao W, Furdui CM. Effects of ionizing radiation on biological molecules—mechanisms of damage and emerging methods of detection. *Antioxid Redox Signal*. 2014;21:260–92.
23. Ferreira CA, Ni D, Rosenkrans ZT, Cai W. Scavenging of reactive oxygen and nitrogen species with nanomaterials. *Nano Res*. 2018;11:4955–84.
24. Liu Y, Li Q, Zhou L, Xie N, Nice EC, Zhang H, Huang C, Lei Y. Cancer drug resistance: redox resetting renders a way. *Oncotarget*. 2016;7:42740–61.
25. Penninckx S, Heuskin A-C, Michiels C, Lucas S. Gold Nanoparticles as a potent radiosensitizer: a transdisciplinary approach from physics to patient. *Cancers*. 2020;12:2021.
26. Daems N, Penninckx S, Nelissen I, Van Hoecke K, Cardinaels T, Baatout S, Michiels C, Lucas S, Aerts A. Gold nanoparticles affect the antioxidant status in selected normal human cells. *Int J Nanomed*. 2019;14:4991–5015.
27. Penninckx S, Heuskin A-C, Michiels C, Lucas S. Thioredoxin reductase activity predicts gold nanoparticle radiosensitization effect. *Nanomaterials*. 2019;9:295.
28. Javvadi P, Herten L, Kosoff R, Datta T, Kolev J, Mick R, Tuttle SW, Koumenis C. Thioredoxin reductase-1 mediates curcumin-induced radiosensitization of squamous carcinoma cells. *Can Res*. 2010;70:1941–50.
29. Kshattray S, Saha A, Gries P, Tiziani S, Stone E, Georgiou G, DiGiovanni J. Enzyme-mediated depletion of l-cyst(e)ine synergizes with thioredoxin reductase inhibition for suppression of pancreatic tumor growth. *Npj Precis Oncol*. 2019;3:16.
30. Rajamanickam V, Yan T, Wu L, Zhao Y, Xu X, Zhu H, Chen X, Wang M, Liu Z, Liu Z, et al. Allylated curcumin analog CA6 inhibits TrxR1 and leads to ROS-dependent apoptotic cell death in gastric cancer through Akt-FoxO3a. *Cancer Manag Res*. 2020;12:247–63.
31. Penninckx S, Heuskin A-C, Michiels C, Lucas S. The role of thioredoxin reductase in gold nanoparticle radiosensitization effects. *Nanomedicine*. 2018;13:2917–37.
32. Miao L, Holley AK, Zhao Y, St Clair WH, St Clair DK. Redox-mediated and ionizing-radiation-induced inflammatory mediators in prostate cancer development and treatment. *Antioxid Redox Signal*. 2014;20:1481–500.
33. Kim KS, Lee D, Song CG, Kang PM. Reactive oxygen species-activated nanomaterials as theranostic agents. *Nanomedicine (Lond)*. 2015;10:2709–23.
34. Smith TA, Kirkpatrick DR, Smith S, Smith TK, Pearson T, Kailasam A, Herrmann KZ, Schubert J, Agrawal DK. Radioprotective agents to prevent cellular damage due to ionizing radiation. *J Transl Med*. 2017;15:232.
35. Liang P-S, Haff RP, Ovchinnikova I, Light DM, Mahoney NE, Kim JH. Curcumin and quercetin as potential radioprotectors and/or radiosensitizers for x-ray-based sterilization of male navel orangeworm larvae. *Sci Rep*. 2016;2019:9.
36. Jagetia GC, Venkatesha VA, Reddy TK. Naringin, a citrus flavonone, protects against radiation-induced chromosome damage in mouse bone marrow. *Mutagenesis*. 2003;18:337–43.
37. Nair GG, Nair CKK. Radioprotective effects of gallic acid in mice. *Biomed Res Int*. 2013;2013:953079–953079.
38. Ghelishli N, Ghasemi A, Hosseinimehr SJ. The influence of piperine on the radioprotective effect of curcumin in irradiated human lymphocytes. *Turk J Pharm Sci*. 2019;16:366–70.
39. Jagetia GC. Radioprotection and radiosensitization by curcumin. In: Aggarwal BB, Surh Y-J, Shishodia S, editors. *The molecular targets and therapeutic uses of curcumin in health and disease*. Boston: Springer; 2007. p. 301–20.
40. Garg AK, Buchholz TA, Aggarwal BB. Chemosensitization and radiosensitization of tumors by plant polyphenols. *Antioxid Redox Signal*. 2005;7:1630–47.
41. Kaur R, Khullar P, Mahal A, Gupta A, Singh N, Ahluwalia GK, Bakshi MS. Keto-enol tautomerism of temperature and pH sensitive hydrated curcumin nanoparticles: their role as nanoreactors and compatibility with blood cells. *J Agric Food Chem*. 2018;66:11974–80.
42. Manimaran S, SambathKumar K, Gayathri R, Raja K, Rajkamal N, Venkatachalapathy M, Ravichandran G, Lourdu EdisonRaj C. Medicinal plant using ground state stabilization of natural antioxidant curcumin by keto-enol tautomerisation. *Natl Prod Bioprospect*. 2018;8:369–90.

43. Tawfik SS, Abouelella AM, Shahein YE. Curcumin protection activities against  $\gamma$ -Rays-induced molecular and biochemical lesions. *BMC Res Notes*. 2013;6:375.
44. Boretti A: Evidence for the use of curcumin in radioprotection and radiosensitization. *Phytotherapy Res* 2023, n/a.
45. Nosrati H, Danafar H, Rezaeejam H, Gholipour N, Rahimi-Nasrabadi M. Evaluation radioprotective effect of curcumin conjugated albumin nanoparticles. *Bioorg Chem*. 2020;100: 103891.
46. Ching YC, Gunathilake TMSU, Chuah CH, Ching KY, Singh R, Liou N-S. Curcumin/Tween 20-incorporated cellulose nanoparticles with enhanced curcumin solubility for nano-drug delivery: characterization and in vitro evaluation. *Cellulose*. 2019;26:5467–81.
47. Chapman JD, Reuvers AP, Borsa J, Greenstock CL. Chemical radioprotection and radiosensitization of mammalian cells growing in vitro. *Radiat Res*. 1973;56:291–306.
48. Grégoire V, Beauvain M, Rosier JF, De Coster B, Bruniaux M, Octave-Prignot M, Scalliet P. Kinetics of mouse jejunum radiosensitization by 2',2'-difluorodeoxycytidine (gemcitabine) and its relationship with pharmacodynamics of DNA synthesis inhibition and cell cycle redistribution in crypt cells. *Br J Cancer*. 1997;76:1315–21.
49. Redpath JL, Willson RL. Reducing compounds in radioprotection and radio-sensitization: model experiments using ascorbic acid. *Int J Radiat Biol Relat Stud Phys Chem Med*. 1973;23:51–65.
50. Lv S, Long W, Chen J, Ren Q, Wang J, Mu X, Liu H, Zhang X-D, Zhang R. Dual pH-triggered catalytic selective Mn clusters for cancer radiosensitization and radioprotection. *Nanoscale*. 2020;12:548–57.
51. Yadav P, Bandyopadhyay A, Chakraborty A, Sarkar K. Enhancement of anticancer activity and drug delivery of chitosan-curcumin nanoparticle via molecular docking and simulation analysis. *Carbohydr Polym*. 2018;182:188–98.
52. Yadav P, Bandyopadhyay A, Chakraborty A, Islam SM, Sarkar K. Enhancing the radiotherapeutic index of gamma radiation on cervical cancer cells by gold nanoparticles. *Gold Bull*. 2019;52:185–96.
53. Rydberg B. Clusters of DNA damage induced by ionizing radiation: formation of short DNA fragments. II Experimental detection. *Radiat Res*. 1996;145:200–9.
54. Mladenova V, Mladenov E, Stuschke M, Iliakis G. DNA damage clustering after ionizing radiation and consequences in the processing of chromatin breaks. *Molecules*. 2022;27:1540.
55. van Leeuwen CM, Oei AL, Crezee J, Bel A, Franken NAP, Stalpers LJA, Kok HP. The alfa and beta of tumours: a review of parameters of the linear-quadratic model, derived from clinical radiotherapy studies. *Radiat Oncol*. 2018;13:96.
56. Ritter M. Rationale, conduct, and outcome using hypofractionated radiotherapy in prostate cancer. *Semin Radiat Oncol*. 2008;18:249–56.
57. Dang CV. MYC on the path to cancer. *Cell*. 2012;149:22–35.
58. Meyer N, Penn LZ. Reflecting on 25 years with MYC. *Nat Rev Cancer*. 2008;8:976–90.
59. Wade MA, Sunter NJ, Fordham SE, Long A, Masic D, Russell LJ, Harrison CJ, Rand V, Elstob C, Bown N, et al. c-MYC is a radiosensitive locus in human breast cells. *Oncogene*. 2015;34:4985–94.
60. Miller DM, Thomas SD, Islam A, Muench D, Sedoris K. c-Myc and cancer metabolism. *Clin Cancer Res Off J Am Assoc Cancer Res*. 2012;18:5546–53.
61. Vafa O, Wade M, Kern S, Beeche M, Pandita TK, Hampton GM, Wahl GM. c-Myc can induce DNA damage, increase reactive oxygen species, and mitigate p53 function: a mechanism for oncogene-induced genetic instability. *Mol Cell*. 2002;9:1031–44.
62. Juin P, Hueber AO, Littlewood T, Evan G. c-Myc-induced sensitization to apoptosis is mediated through cytochrome c release. *Genes Dev*. 1999;13:1367–81.
63. Hassan F-u, Rehman MS-u, Khan MS, Ali MA, Javed A, Nawaz A, Yang C. Curcumin as an alternative epigenetic modulator: mechanism of action and potential effects. *Front Genet*. 2019;10:514.
64. Banerjee S, Ji C, Mayfield JE, Goel A, Xiao J, Dixon JE, Guo X. Ancient drug curcumin impedes 26S proteasome activity by direct inhibition of dual-specificity tyrosine-regulated kinase 2. *Proc Natl Acad Sci*. 2018;115:8155–60.
65. Demšar J, Curk T, Erjavec A, Gorup Č, Hočevar T, Milutinovič M, Možina M, Polajnar M, Toplak M, Starič A. Orange: data mining toolbox in Python. *J Mach Learn Res*. 2013;14:2349–53.
66. Szklarczyk D, Gable AL, Lyon D, Junge A, Wyder S, Huerta-Cepas J, Simonovic M, Doncheva NT, Morris JH, Bork P, et al. STRING v11: protein-protein association networks with increased coverage, supporting functional discovery in genome-wide experimental datasets. *Nucleic Acids Res*. 2019;47:D607–13.
67. Khatrı P, Sirota M, Butte AJ. Ten years of pathway analysis: current approaches and outstanding challenges. *PLoS Comput Biol*. 2012;8:e1002375–e1002375.
68. Glazko GV, Emmert-Streib F. Unite and conquer: univariate and multivariate approaches for finding differentially expressed gene sets. *Bioinformatics*. 2009;25:2348–54.

**Publisher's Note** Springer Nature remains neutral with regard to jurisdictional claims in published maps and institutional affiliations.